A&A 374, 265–279 (2001)
DOI: 10.1051/0004-6361:20010735

Astronomy & Astrophysics

LTE spectrum synthesis in magnetic stellar atmospheres

The interagreement of three independent polarised radiative transfer codes

G. A. Wade[1], S. Bagnulo[2,3], O. Kochukhov[4], J. D. Landstreet[5], N. Piskunov[4], and M. J. Stift[2]

[1] Département de Physique, Université de Montréal, CP 6128 succ. Centre-Ville, Montréal, QC, Canada H3C 3J7
[2] Institut für Astronomie, Universität Wien, Türkenschanzstr. 17, 1180 Wien, Austria
[3] European Southern Observatory, Casilla 19001, Santiago 19, Chile
[4] Uppsala Astronomical Observatory, Box 515, 751 20 Uppsala, Sweden
[5] Physics & Astronomy Department, University of Western Ontario, London, Ontario, Canada N6A 3K7

Received 10 November 2000 / Accepted 22 May 2001

Abstract. With the aim of establishing a benchmark for the detailed calculation of the polarised line profiles of magnetic stars, we describe an intercomparison of LTE Stokes profiles calculated using three independent, state-of-the-art magnetic spectrum synthesis codes: Cossam, Invers10 and Zeeman2. We find, upon establishing a homogeneous basis for the calculations (identical definitions of the Stokes parameters and the magnetic and stellar reference frames, identical input model stellar atmosphere, identical input atomic data, and identical chemical element abundances and magnetic field distributions), that local and disc-integrated Stokes $IQUV$ profiles of Fe II λ4923.9 calculated using the three codes agree very well. For the illustrative case of disc-integrated profiles calculated for abundance $\log n_{\rm Fe}/n_{\rm tot} = -4.60$, dipole magnetic field intensity $B_{\rm d} = 5$ kG, and projected rotational velocity $v_{\rm e} \sin i = 20$ km s^{-1}, Stokes I profiles (depth ∼40% of the continuum flux $I_{\rm c}$) agree to within about 0.05% rms of $I_{\rm c}$, Stokes V profiles (full amplitude ∼10%) to within about 0.02% rms of $I_{\rm c}$, and Stokes Q and U profiles (full amplitudes ∼2%) at the sub-0.01% rms level. These differences are sufficiently small so as to allow for congruent interpretation of the best spectropolarimetric data available, as well as for any data likely to become available during the near future. This indicates that uncertainties in modeling Stokes profiles result overwhelmingly from uncertainties in input atomic and physical data, especially the state and structure of model stellar atmospheres.

Key words. line: profiles – polarisation – stars: magnetic fields – stars: atmospheres

1. Introduction

Magnetic fields have now been confidently detected in the atmospheres of stars occupying most regions of the H–R diagram: on the pre-main sequence (Donati et al. 1997; Johns-Krull et al. 1999), the lower (Johns-Krull et al. 1996), middle (Babcock 1947, 1958) and upper (Bohlender et al. 1987) main sequence, among evolved stars (Donati et al. 1997), and among degenerate objects (Kemp et al. 1973). In order to study the detailed structure and the origins of these fields, as well as their impact on other physical processes operating in stellar atmospheres, accurate calculations of spectral line profiles modified by the Zeeman effect are necessary. Of particular diagnostic value are the variations of circular and linear polarisation across spectral lines, often referred to as the Stokes QUV profiles. Recently, the first high-precision time-resolved observations of all the Stokes profiles of magnetic stars were reported (Wade et al. 2000). Interpretation of these new data requires the ability to confidently calculate synthetic Stokes profiles.

Spectrum synthesis for magnetic stars involves all the intricacies of unpolarised spectrum synthesis – accurate atomic data, model atmospheres, continuous opacities, and line opacities, consideration of relevant broadening mechanisms, non-LTE effects, etc., plus a number of other factors associated with the particular problems of magnetic fields and polarised light: consistent definitions of the Stokes parameters, magnetic field configuration and stellar model geometry, accurate summation of the local Stokes $IQUV$ profiles over the visible stellar disc, and additional atomic data (Landé factors and the intensities of Zeeman components). In addition, because the amplitudes of the Stokes profiles of magnetic stars are often very weak (of order 1% of the continuum flux) the requisite accuracy of the calculation is substantially more stringent than

Send offprint requests to: G. A. Wade,
e-mail: wade@astro.umontreal.ca

is usually required for unpolarised synthesis. Finally, polarised spectrum synthesis requires a much larger number of calculations than does unpolarised synthesis, increasing the computational demand and requiring faster hardware and/or more efficient coding.

The existence of these intricacies implies that the potential exists for substantial differences among independent calculations of synthetic Stokes profiles. In this paper we describe a careful intercomparison of Stokes profiles calculated using three independent polarised spectrum synthesis codes, with the aim of quantifying their agreement, establishing a benchmark for future calculations, and identifying the main sources of uncertainty. Our goal is to answer the question: how similar are the Stokes profiles calculated by each of the three codes, under identical input conditions (i.e. identical model stellar atmosphere, atomic data)? As a secondary goal we examine the sensitivity of the calculated profiles to changes in the input conditions. In Sect. 2 we introduce the three synthesis codes, and in Sect. 3 we establish a consistent astrophysical basis for the comparison. In Sect. 4 we describe an extensive series of tests designed to evaluate the agreement among local and disc-integrated synthetic Stokes profiles, and in Sect. 5 we discuss the dependence of this agreement on changes in the input conditions, and summarise our findings.

2. An introduction to three PRT codes

Modeling the spectral line profiles of non-magnetic stars in LTE requires the solution of the unpolarised radiative transfer problem, which involves a single first-order linear differential equation. Treatment of the spectral lines of magnetic stars in LTE, on the other hand, requires the solution of a set of four coupled first-order linear differential equations, one for each Stokes parameter[1] (e.g. Rees 1987). The practical problem of computing the solution to this system of equations is the polarised radiative transfer, or PRT, problem.

2.1. COSSAM

Cossam stands for "**Co**dice per la **s**intesi **s**pettrale nelle **a**tmosfere **m**agnetiche". It is the first object-oriented parallel code in the field of (polarised) spectral line synthesis and is the result of a major software engineering effort. Cossam is designed for the accurate direct calculation of full Stokes $IQUV$ spectra in the sun or in rotating and/or pulsating stars whose magnetic fields are represented by a tilted, eccentric dipole, or by a dipole-quadrupole expansion.

[1] All three magnetic spectrum synthesis codes discussed in this paper employ identical definitions of the Stokes parameters which conform to that developed by Shurcliff (1962).

2.1.1. A short history

Genealogists won't find it difficult to trace Cossam back to the Algol 60 code *Analyse 65* by Baschek et al. (1966) and its Fortran adaptation ADRS (Peytremann et al. 1967). An evolved version ADRS3 by Chmielewski (1979) was modified by Stift (1985) in order to synthesise Stokes I and V profiles in rotating and/or pulsating magnetic stars. Restricting the scope of the code to the synthesis of a single Zeeman-split line with an arbitrarily complex Zeeman pattern in intensity and circular polarisation made it possible to employ the fast polarised formal solver given in Hardorp et al. (1975); the systematic investigation of theoretical Stokes V profiles for magnetic stars was made feasible on a VAX 11/750.

The study of broadband linear polarisation (BBLP) in CP stars by Landolfi et al. (1993) made it clear that, in order to investigate and exploit the full diagnostic contents of BBLP, there was an urgent need for a code that could synthesise full Stokes profiles in (heavily) blended spectra. An attempt to modify the existing Fortran-77 code in a way as to be able to calculate full Stokes profiles for blends was abandoned when it emerged that there would be no readable and easily modifiable code without the radical rewriting of the code in a language of less restricted expressive power. The first software design solution for a Stokes code in Ada83 was presented in 1993 more or less in the guise of a Christmas present by a student, G. Könighofer. The convincing design and the impending revision of Ada which promised so many powerful new language features (now all found in Ada95) never left any doubt as to the desirability of exploring object-oriented parallelism with Ada95. Ultimately this has led to the development of a whole family of parallel codes including Cossam, a Zeeman Doppler Imaging code, and Carat, a code for the calculation of radiative accelerations in magnetic atmospheres.

2.1.2. Object-orientation and concurrency with Ada95

Polarised spectral line synthesis in the Zeeman regime is not overly complicated from the physical or numerical point of view; the difficulties lie in software engineering issues. The ultimate goal of portability, modifiability, extensive software reuse and parallelism in addition to computational efficiency can only be attained by using a standardised object-oriented language with parallel constructs (see Stift 1998a, for an introduction and code examples).

A *data type* is characterised by a set of values and a set of operations that can be applied to those values. There is no implicit type conversion in Ada95, in contrast to Fortran. This *strong typing* implies that values of one type cannot be assigned to variables of another type, enabling incredibly extensive static compiler checks.

Values can be stored in *objects*, declared to be of a specific type. Each *type declaration* introduces a new type totally distinct from any other type; it subsequently has to be *exported* (made visible) to other software modules.

Data types can be of almost arbitrary complexity (see e.g. Stift 1996).

Efficient "programming in the large" must be based on truly reusable software components ("verbatim reuse"). The use of abstract data types, encapsulation, information hiding, generics, inheritance and programming by extension is essential for this purpose; we may loosely designate it as object-orientation.

A large program – such as COSSAM – builds on numerous user-defined data types and many subprograms. Type definitions and their associated operations can be *encapsulated* in packages, and it is also often useful to group together related subprograms in packages. In order to facilitate software reuse, packages (and subprograms) can be *parameterised*. *Generic packages* are *templates* with *formal parameters* which have to be *instantiated* with *actual parameters*.

Any extension to a package which is used in many different programs will lead to the necessity of recompiling all programs that use this package; it may also introduce new bugs in a well tested, trusted software component. Ada95 allows "incremental programming": you can extend existing packages without recompilation. *Child units* have full access to all the declarations and subprograms in their ancestors. Types and subprograms can be *overloaded*, i.e. replaced by alternative ones of the same name.

In contrast to High Performance FORTRAN, Ada95 provides thread-parallel *task* constructs. Tasks are program entities that perform a sequence of actions and that can execute *concurrently* within the same program on several processors. Tasks are declared as *task objects* and start to execute upon *elaboration* of the object declaration; each task has its own *thread of control*.

Protected objects, which do not have a thread of control of their own, are accessed in *mutual exclusion*, i.e. only one process can update a variable at a time. In the *rendezvous* mechanism a task can call an *entry* of another task or *accept* a call on one of its own entries. Protected objects and the rendezvous are used for synchronisation between task and calling program, or between different tasks.

2.1.3. The underlying physics and numerics

COSSAM works under the assumption of LTE in a plane-parallel atmosphere. The atomic transitions are taken from the VALD database (Piskunov et al. 1995). The atomic partition functions are normally calculated with the Kurucz (1993) routine rewritten in Ada95, but one can also choose those by Traving et al. (1966), Irwin (1981), or Cowley (1998). In the Saha equation the lowering of the ionisation potential as a function of temperature and electron density is taken into account. Radiation damping, Stark broadening and van der Waals broadening constants are taken from VALD. When experimental constants are unavailable, classical radiation damping and Unsöld van der Waals broadening respectively are assumed, and Stark broadening can be ignored or approximated according to Gonzalez et al. (1995).

The Zeeman splitting and component strengths are calculated with the help of the Landé factors and J-values of the respective lower and upper energy levels provided by VALD. A classical Zeeman-triplet is assumed whenever Landé factors are missing. Partial Paschen-Back effect is not taken into account.

For the continuous opacity κ_λ at a given wavelength, COSSAM interpolates in a 2D table (wavelength – depth) provided by ATLAS 9 (Kurucz 1993). The total line opacities required in the formal solver are determined by full opacity sampling of the σ_-, the σ_+, and π components separately.

For metallic lines, COSSAM employs the rational approximation to the Voigt and Faraday functions given in Landolt-Börnstein (1982). The hydrogen line profiles are calculated by interpolation in the tables given by Stehlé & Hutcheon (1999). As to the polarised formal solver, the user has the choice between the Zeeman Feautrier method (Auer et al. 1977) and the somewhat faster but less accurate DELO method (Rees et al. 1989). Magneto-optical effects are normally included in the formal solution but there is a runtime option to suppress them.

In the "solar case" (local case) the emerging spectrum is calculated for one given point (with a given magnetic vector) on the solar surface, whereas in the "stellar case" (disc-integrated case), COSSAM integrates the emerging spectrum over the visible hemisphere, taking into account rotation, (non)radial pulsation and global (dipolar and/or quadrupolar) magnetic field structure. A special algorithm discussed by Stift (1985) and Fensl (1995) provides an optimum grid for this 2D-integration, thereby greatly reducing the number of quadrature points required in comparison to fixed grids.

2.1.4. Transportability

Task types and protected types are part of the Ada95 kernel language, so COSSAM is perfectly transportable from any PC to a 512-processor supercomputer: exactly 2 lines of code have to be changed! No message passing libraries, no need to delve into pthread-programming, no extra software to be bought and/or installed. And there is a public version of COSSAM which is free software, available for many platform/operating system combinations; you can redistribute it and/or modify it under the terms of the GNU General Public License as published by the Free Software Foundation. Source code, data files and documentation can be downloaded from:

`http://fedelma.astro.univie.ac.at/web/cossam/index.html`

2.2. INVERS10

INVERS10 is a Magnetic Doppler Imaging code designed for reconstructing the distribution of magnetic field

vectors and abundance of one chemical element over the surface of magnetic Ap stars. The maps are recovered from a time series of the spectropolarimetric observations by solving a regularised inverse problem.

The core of INVERS10 is a magnetic spectrum synthesis code that solves the equation of radiative transfer for four Stokes parameters for all visible elements on the stellar surface, and performs disc integration to simulate the observed Stokes spectra. We have implemented two transfer algorithms: magnetic (or Zeeman) Feautrier and Diagonal Element Lambda Operator (DELO). Both algorithms have advantages and problems and the final choice is unclear at this stage.

The Feautrier method is well-established as a fast and very stable radiative transfer solver for non-magnetic synthesis. Therefore, it was logical to extend it to the case of magnetic synthesis. Such an algorithm was first formulated by Auer et al. (1977). Similar to conventional Feautrier, the vector of Stokes parameters throughout the atmosphere is found by solving a system of linear equations with the right-hand side dependent upon the source function and with a block tri-diagonal matrix. Each matrix element consists of a 4×4 block dependent upon the total opacity matrix. The magneto-optical effects are included as cross-terms between the Q, U and V Stokes parameters in the opacity matrix. During the course of multiple tests we discovered that the primary advantages of the Feautrier techniques (stability and rapid convergence) are preserved in the magnetic case. On the other hand, we found a problem with numerical stability caused by the fact that the opacity matrix K can become nearly degenerate. This happens, for example, for a strong magnetic field in the the cores of Zeeman sigma components (Piskunov 1999). The solution is to use matrix pivoting when inverting the opacity matrices, a procedure that is costly in terms of computing time (factor of 2).

The alternative DELO method suggested by Rees et al. (1989) replaces the opacity matrix with so-called pseudo-opacity matrix in which the diagonal is always dominant. The formal solution of the radiative transfer equation at each tabulated atmospheric depth is evaluated analytically assuming a linear depth dependence of the source function. This allows the construction of a one-way integrator for the Stokes parameters. At each integration step this requires the inversion of a single 4×4 matrix, which can be performed very efficiently without pivoting. For a modern super-scalar workstation that translates into 2.5 times speed increase compared to Feautrier. Unfortunately, the convergence properties (the decrease of residual errors with the number of vertical integration steps) is noticeably worse than for Feautrier. For this reason the Feautrier version of INVERS10 was used for all the tests in this paper.

The calculations of the opacity matrix and the source function assume LTE and an unpolarised continuum. The code is capable of calculating synthetic spectrum over several wavelength intervals by combining the opacity matrices of individual lines and interpolating the continuum intensities between the two ends of each interval. The calculations of continuous opacities and partition functions are adapted from the ATLAS9 code (Kurucz 1993), with the exception of rare earth elements for which the partition functions were provided by Cowley (1998).

The main purpose of INVERS10 is to solve the inverse problem, which means reconstructing the magnetic vector and abundance value at each point on the visible stellar surface. This goal requires that the implementation of the radiative transfer solver be both fast and accurate. We have separated the program in two parts. The main part performs input/output, constructs the surface grid and pre-calculates the line opacities and damping in the center of each line throughout all atmospheric layers. We assume the same atmosphere model to be suitable for all surface elements and the abundance/magnetic field vector to be constant within each element (both horizontally and vertically). The main program also performs disc integration and adjustment of the abundance and magnetic field values based on comparison with the observations.

The surface grid employs fixed steps in latitude and variable steps in longitude that preserve approximately the area of surface elements. The radiative transfer is performed by a separate program (RT solver). Several RT solvers can run in parallel. The main program initialises each RT solver by passing the table of central line opacities and damping parameters. During disc integration the main program passes the local abundances and magnetic field vector, as well the orientation of the surface element relative to the line-of-sight for all rotational phases. After initiating the calculations for the first element the main program continues distributing surface elements to available RT solvers until all are busy. Each RT solver constructs the total opacity matrix and solves the radiative transfer equation for 4 Stokes parameters on an adaptive wavelength grid which ensures accurate linear interpolation between wavelength samples. The calculations are repeated for all rotational phases. Next the polarisation spectra are interpolated onto an equispaced wavelength grid and convolved with the instrumental profile using a Fast Fourier Transform. Finally the spectra are returned to the main program for disc integration.

The main program receives the data from the RT solver that first completes the calculations and restarts that solver with the data for the next surface element in the queue. In this way an automatic load balance is achieved when INVERS10 is used on a multi-CPU machine. The implementation of the RT solver as a separate program allows experimentation with different numerical algorithms without modification to the main component of INVERS10.

The typical size of the surface grid is between 300 and 2500 elements. The disc integration takes into account rotational Doppler shifts for each rotational phase and the transformation of the Q and U Stokes parameters to the observer's frame.

The INVERS10 code can be used for simulating Stokes parameters for a star with arbitrary field and surface

abundance distribution geometry (forward mode) or for Magnetic Doppler Imaging (inverse mode). For inverse mode, high-quality spectropolarimetric observations for different rotational phases are required. Based on numerical experiments, typically 30–40 iterations are required to reconstruct both the magnetic field and abundance maps. For smooth global fields we have developed a special type of multipolar regularization that allows the use of a limited dataset (only Stokes I and V) (Piskunov & Kochukhov 2000, in preparation).

2.3. ZEEMAN2

ZEEMAN2 is the descendant of the original FORTRAN-77 LTE line synthesis code ZEEMAN, described by Landstreet (1988). The code is designed both for direct calculation of polarised spectra and for modeling of data using a simple field description and a simply parametrised element distribution.

Here we provide a short history of the code and the motivation for its development, and a description of its internal workings, especially its scheme for integration of the polarised transfer equations.

2.3.1. Historical motivation

In the early 1980's it was clear that interest in obtaining Doppler abundance maps of magnetic Ap stars was increasing. However, mapping was focussed on reconstructing equivalent width distributions in stars with particularly weak fields, so that simple local line profiles could be used. Therefore mapping was moving in the direction of studying precisely the stars for which one knows the least about the magnetic geometry. From the point of view of clarifying what diffusion theory has to explain, this seemed relatively unhelpful. In fact, the most interesting stars to model are the ones for which one has the maximum of information about *both* the field and the abundance patches. But clearly to model these stars one must be able to model strongly magnetically-split lines.

The intention of ZEEMAN was never to do detailed magnetic or abundance mapping, but rather to obtain approximate models of *both* magnetic field and abundance distributions for a few stars at a level of detail suitable for comparison with diffusion theory. It was decided from the outset to try to include as much physics as was affordable, so as to have reasonable confidence that the synthesis was physically reasonable. However, the slowness and cost of computers made forward integration only (and small arrays and mimimal CPU time) a necessity. It was planned initially to make comparisons by eye and to adjust by hand; this was the procedure used by Landstreet (1988) in modeling 53 Cam. However, after initial experiments indicated that ZEEMAN ran some 50 (!) times faster on a Cray than on a Cyber 835, the potential for automatic fitting became clear and the code was modified to allow for control by a least-squares optimisation routine. The subroutine responsible for integration of the transfer equations was also rewritten to allow it to vectorise on the Cray (another gain of 4× in speed).

Besides the standalone line synthesis version of ZEEMAN2 (which is capable of producing Stokes $IQUV$ spectra for both the local and disc-integrated cases) used for the calculations reported in this paper, ZEEMAN2 is currently incorporated into a suite of tools for modeling (in the simple ZEEMAN tradition) horizontal abundance nonuniformities, vertical abundance stratification, and radial pulsation simultaneously with recovery of the axisymmetric multipolar magnetic field geometry, using observations in all 4 Stokes parameters.

2.3.2. Integration of the transfer equations

To numerically integrate the polarised transfer equations, both ZEEMAN and ZEEMAN2 employ the efficient quasi-analytic technique proposed by Martin & Wickramasinghe (1979). This technique assumes that the coupled transfer equations have constant coefficients between successive tabulated atmospheric depths, so that the analytic Unno-Rachkovsky solution may be used at depth m in the atmosphere to calculate the values of the Stokes parameters from values at depth $m + 1$. This technique is essentially as accurate as, and is much faster than, direct integration of the transfer equations.

Martin & Wickramasinghe present two general solutions to the transfer problem: the "restricted" solution for 3 Stokes parameters ignoring anomalous dispersion, and the "full" solution for 4 Stokes parameters including anomalous dispersion. With the expectation that anomalous dispersion would not strongly affect the calculated Stokes profiles (and Stokes I in particular), Landstreet (1988) adopted the "restricted" solution; this solution requires about 50% less time for execution than does the "full" solution[2].

The most fundamental difference between ZEEMAN and ZEEMAN2 involves the inclusion of anomalous dispersion in the solution to the polarised transfer equations, accomplished by substituting the 4 Stokes parameter solution of Martin & Wickramasinghe for their 3 Stokes parameter solution. This turned out to be a highly nontrivial exercise: even for the relatively simple 3 Stokes parameter solution, Landstreet (1988) found that in the special case where the line absorption coefficients η_V and η_Q vanish, the transfer equations decouple and a special subsolution (Landstreet 1988) must be employed. In the case of the 4 Stokes parameter solution, the potential for decoupling increases manyfold, and 9 independent subsolutions (including the "full" solution and the "restricted" solution as special cases) are required. It was necessary to derive these subsolutions in order to implement the 4 Stokes

[2] In fact we find that anomalous dispersion can be critically important for determining the profile shapes of *all* Stokes parameters, including Stokes I. This will be discussed in a future publication.

parameter transfer solution in ZEEMAN2. Details regarding the particular pathologies and requisite subsolutions of the Martin & Wickramasinghe 4 Stokes solution can be obtained by contacting JDL.

2.3.3. Physical foundations

ZEEMAN2 employs pretabulated plane-parallel atmosphere models (e.g. ATLAS models). Atomic data is extracted from various sources (usually the VALD database), and Zeeman patterns are calculated using the L, S and J quantum numbers characterising the upper and lower levels of the transitions to calculate splitting and Landé factors (assuming LS coupling). Partition functions are calculated from polynomial approximations taken from Bolton (1970, 1971) for elements up to Zr, and from Aller & Everett (1972), Cowley & Adelman (1983) and Cowley (1994) for more massive elements, and partition functions from Irwin (1981) are also available. Ionic populations are calculated for (up to) the fourth ionisation state (i.e. up to state $iv \equiv +3$) using the Saha equation. Radiation damping, van der Waals broadening and quadratic Stark broadening are each taken into account, usually using constants supplied from the literature (usually VALD), and otherwise classical radiation damping and the Unsöld approximation for van der Waals broadening are assumed. Quadratic Stark effect is otherwise calculated using the approximation described by Cowley (1971) for neutrals, and the approximation of Griem (1968) as simplified and empirically recalibrated by Gonzalez et al. (1995) for ions broadened by electrons.

ZEEMAN2 does not presently calculate lines of He or H (although implementation is currently underway). Metallic line opacity and anomalous dispersion profiles are described assuming the Voigt $H(a, v)$ and Faraday-Voigt $F(a, v)$ functions calculated using the numerical recipe by Humlicek (1982). We note that the Faraday-Voigt function produced using this formulation implicitly includes a factor of 2, i.e. it in fact results in $2\,F(a, v)$.

Continuous opacities are calculated for H I, H^-, He I bound-free (b-f) and free-free (f-f) transitions, Rayleigh scattering by H I and electron scattering (both treated as absorption). H I b-f Gaunt factors are from Carbon & Gingerich (1969), while those for H I f-f are calculated from the Menzel-Pekeris approximation (as quoted by Gray 1992). H^- b-f and f-f are calculated from the polynomial fits by Gingerich (1964), which give results similar to those reported by Gray (1992). He I b-f and f-f opacities are calculated using a hydrogenic approximation, as discussed briefly by Gingerich (1964) and Mihalas (1970). Rayleigh scattering by H I is calculated using an expression from Dalgarno quoted by Gingerich (1964).

The magnetic field is described as a oblique axisymmetric linear multipole including terms up to the octupole. Departures from axisymmetry can be introduced by multiplying such an axisymmetric field distribution by a series of spherical harmonics consistent with those employed in the modeling by Leroy et al. (1996).

At each rotational phase, the visible stellar disc is divided into anywhere from about 60 up to several thousand subelements of approximately equal projected area (Landstreet 1988), and in each subelement the transfer equations are integrated vertically through the atmosphere for the specific local abundance and magnetic field (assumed constant both vertically and horizontally in each subelement) to yield the surface Stokes intensities $I(\lambda), V(\lambda), Q(\lambda), U(\lambda)$. Because the transfer calculation occurs in the frame of reference of the surface subelement, the surface intensities can be summed for Doppler shifts corresponding to various macroscopic velocity fields (in particular projected rotational velocities, $v_{\rm e} \sin i$) before convolution with the (assumed Gaussian) instrumental profile.

2.4. Parallelism, load balance and Amdahl's law

Spectral line synthesis is an "embarrassingly parallel" problem. Sampling the opacity, solving the transfer equation, and integrating the local Stokes parameters over the stellar disc can be carried out in parallel for all line frequencies.

INVERS10 is written in FORTRAN-77, and the communication between the main program and the RT solvers is based on the Message Passing Interface (MPI). MPI is available as a public domain library as well as proprietary packages for all major brands of high-performance computers.

COSSAM, developed in Ada95, relies on light-weight synchronisation by means of protected objects which provide exclusive read-write access or concurrent read-only access to shared data. For more details on concurrency and synchronisation with Ada95 in the context of astrophysics the reader is referred to Stift (1998b).

Gene Amdahl in 1967 postulated that there is a maximum speedup that can be achieved by using many processors in parallel processing. Since the nature of the synchronisation overhead in parallelism appears to be sequential, the maximum speedup that can be achieved by using P processors is given by $1/(F + (1 - F)/P)$ where F is the fraction of a calculation that is sequential (essentially synchronisation). This is known as Amdahl's law.

The *granularity* of the parallel calculations by INVERS10 or COSSAM determines when Amdahl's law becomes important. Several choices are possible which depend on the way the supercomputer facilities are organised.

In Uppsala, on a Hewlett Packard V2500 server and a Cray T3E with up to 128 CPUs, INVERS10 is run on a number of CPUs which are also used by other jobs. Thus the available resources are constantly changing. The parallelisation scheme has to be capable of always using all currently available resources; we may refer to this as "dynamic load balance". Even when the various individual

processes do not finish at the same time, there is no waste of resources thanks to the other users. It is therefore possible to employ *coarse-grained* parallelism: INVERS10 distributes calculations related to individual disc surface elements among the available processors, so synchronisation can take place only after a full local Stokes profile has been calculated. With F as low as 10^{-4} or 10^{-5}, linear scaling is fulfilled up to a few hundred CPUs.

COSSAM and CARAT, a code to calculate radiative accelerations, have been devised to run on supercomputers of the SGI Origin family. With the "Miser" deterministic batch scheduling facility a fixed number of CPUs must be reserved. It is imperative to achieve almost perfect load balance among the various Ada taks to avoid waste of resources allocated exclusively to the job. This implies a more *fine-grained* parallelism. COSSAM and CARAT distribute 1 Å wavelength intervals rather than surface elements. Although only 1 protected is necessary for synchronisation purposes, the value of F can go up to around 10^{-3}. Amdahl's law then implies that it does not make sense to use more than typically 64 CPUs. Note that this fine-grained parallelism will also achieve perfect load-balance on systems where CPUs are not allocated exclusively to a single user.

Summarising this discussion, we want to emphasise that there is no single optimum approach to parallelism, not even in the restricted field of (polarised) spectrum synthesis. It is relatively easy to obtain near perfect load balance. The number of CPUs up to which speedup is linear depends on the granularity of the approach, is given by Amdahl's law, and strongly depends on how the supercomputing facility is organised.

3. Establishing a consistent framework

As stated in the introduction, our goal is to examine the agreement of the Stokes profiles calculated by the three codes under *identical input conditions*. This requires that we ensure the consistency of the stellar model geometry, as well as the input model atmosphere and input atomic data upon which each code relies. Once this has been established we can begin to explore the level of agreement of the additional data calculated implicitly by each code (atomic and ionic populations, line and continuous opacities) which are furthermore required for the radiative transfer calculation. This procedure will aid in establishing the source of any differences between the Stokes profiles calculated by the codes.

3.1. Stellar model geometry

The calculation of Stokes profiles in the disc-integrated case presents some obvious complications with respect to the local case. The radiative transfer problem must be solved on a two-dimensional spatial grid, which multiplies manyfold the computational expense of the calculation. As well, definitions of the (complex) stellar geometry and magnetic field configuration are required. In fact, for the non-magnetic case, when gravity-darkening is not significant, the projected equatorial rotational velocity $v_{\rm e}\sin i$ is the only parameter required to account for the stellar orientation and rotational velocity. By contrast, in the magnetic case, particular attention must be devoted to provide an unambiguous description of both the orientation of the star's rotation axis and the magnetic field configuration. The photospheres of many magnetic Ap stars are permeated by a relatively smooth magnetic field, usually not symmetric about the rotational axis. A magnetic dipole, tilted with respect to the rotational axis, represents a natural first approximation for the magnetic morphology of this class of stars. Hence, we decided to adopt this simple example of the oblique rotator model (ORM) as representative of many real cases of astrophysical interest. A full characterisation of the dipolar ORM requires six parameters. Three of them specify the orientation of the star's rotation axis, and its rotational velocity:

- the tilt angle of the rotation axis i ($0^\circ \leq i \leq 180^\circ$), counted from the line of sight e_z toward the *positive* rotational pole (see Landolfi et al. 1993 for further details)[3];
- the azimuth angle Θ ($0^\circ \leq \Theta \leq 360^\circ$) of the rotation axis, counted positive from e_x toward e_y in the (e_x, e_y) plane of the reference system adopted for the measurement of the Stokes profiles[4]. It has become conventional to define the reference frame such that the e_x axis is oriented along the North Celestial Meridian (e.g., Landolfi et al. 1993; Leroy 1995; Wade et al. 2000);
- the equatorial rotational velocity $v_{\rm e}$ ($v_{\rm e} \geq 0$), or the more customary projected velocity $v_{\rm e}\sin i$, must also be specified.

The (dipolar) magnetic field configuration is specified by three additional parameters:

- the strength of the dipolar field, usually expressed in terms of field strength at the positive magnetic pole, $B_{\rm p}$;
- the obliquity β ($0^\circ \leq \beta \leq 180^\circ$) of the magnetic dipole axis with respect to the rotation axis, counted from the positive rotational pole toward the positive magnetic pole;
- the rotational phase f ($0^\circ \leq f \leq 360^\circ$); for its detailed definition we refer the reader to Landolfi et al. (1993); in fact, the rotational phase is commonly expressed as a fraction of the rotational cycle, sometimes normalised to 100 (e.g., Leroy 1995), or more often to 1 (e.g., Mathys 1993).

[3] In many astrophysical applications, the inclination of the stellar rotation axis is in the interval $[0^\circ, 90^\circ]$, leaving undetermined the direction in which the star rotates.

[4] Stokes I and V are independent of Θ; Stokes Q and U are invariant under the transformation $\Theta \rightarrow \Theta + 180^\circ$.

3.2. Basic physical data

As a step toward ensuring homogeneity of the input data, we have adopted identical model atmospheres for all spectrum synthesis calculations reported here. The adopted model atmosphere has effective temperature $T_{\rm eff} = 7500$ K, surface gravity (in cgs units) $\log g = 4.0$, solar metallicity, 2 km s^{-1} microturbulence, and has been calculated using ATLAS9 (Kurucz 1993) with standard convection treatment. For this adopted 72-level model, the logarithmic standard optical depth $\log \tau_{5000}$ reaches 0.0 around level 58 (as measured from the top of the atmosphere).

Most line synthesis calculations in this paper are for Fe II λ4923.9. All calculations of this line employ identical transition data. The relevant atomic data has been extracted directly from the VALD database, and is reported in Table 1[5].

Table 1. Atomic data for Fe II λ4923.9, extracted from the VALD database (Piskunov et al. 1995).

λ_0	4923.927 Å
$\log gf$	−1.320
$E_{\rm l}$	2.8910 eV
$E_{\rm u}$	5.4080 eV
$\log \gamma_{\rm rad}$	8.489
$\log \gamma_{\rm stark}$	−6.583
$\log \gamma_{\rm vdW}$	−7.914
lower term	$^6S_{5/2}$
upper term	$^6P_{3/2}$
Lower z	2.00
Upper z	2.40

To furthermore ensure homogeneity of the input data, we have adopted identical partition functions $u(T)$ for Fe II for these tests. The adopted values of $u(T)$ correspond to those reported by Drawin & Felenbock (1965).

In the remainder of this section we employ the three codes, along with this standardised input data, to compare the consistency of the calculated ionic populations and continuous and line opacities.

3.2.1. H and He ion populations

Using the atmosphere model discussed above, the calculated populations of all ionisation states of H and He among the three codes agree to better than 0.01% of the total populations at atmospheric depths above 40, and to better than 0.5% for deeper layers.

[5] Note that although ZEEMAN2 calculates level Landé factors assuming LS coupling, the calculated values for Fe II λ4923.9 are essentially identical to the VALD experimental values.

3.2.2. Continuous opacities

As discussed in Sect. 2, ZEEMAN2 and INVERS10 calculate continuous opacities during execution, while COSSAM adopts opacities output from ATLAS9. In Fig. 1 we compare continuous opacities for the three codes, calculated for the two different sets of physical conditions outlined in Table 2. The agreement for individual source and total opacity appears fairly good on the logarithmic ordinate of Fig. 1. In fact, the total continuous opacities employed by the three codes differ systematically by less than 5% in the visible for the cool conditions, but by about 10% for the hot conditions. In the near infra-red the agreement worsens somewhat. Among individual sources, the electron scattering opacity employed by COSSAM for the hot conditions shows relatively large differences from the other codes' calculations.

Table 2. Physical conditions for the "cool" and "hot" continuous opacity comparisons.

		COOL	HOT
ρ_x	(g cm^{-2})	1.16602898	1.76690304
T	(K)	7042.7	12729.0
$n_{\rm e}$	(cm^{-3})	5.49400E+13	4.14200E+15
$n_{\rm A}$	(cm^{-3})	1.19972E+16	1.00250E+16
ρ	(g cm^{-3})	2.58784E-08	2.16146E-08

3.3. Line opacities

The line opacity η_{IQUV} and anomalous dispersion ρ_{IQUV} are related to the total absorption and anomalous dispersion profiles of the σ and π Zeeman components via the Voigt $H(a, v)$ and Faraday-Voigt $F(a, v)$ functions. Both H and F as calculated by each of the codes agree to within 0.2%.

Differences in the calculated damping a will impact the calculated wings of saturated lines. In Fig. 2 we compare for the three codes radiative, van der Waals and quadratic Stark damping constants calculated for all atmospheric levels for Fe II λ4923.9. The typical spread in total damping is smaller than 1%, although more important systematic differences do exist among the individual damping contributors. The most important systematic difference is associated with the quadratic Stark calculation, where deeper in the atmosphere than level 68 the ZEEMAN2 calculation differs from the others by a maximum of about 10%. Quadratic Stark is the primary damping mechanism in these deepest layers of the atmosphere, and this results in a difference in the ZEEMAN2 total damping below level 68 of about 8% with respect to the others (which maintain agreement to within 1%). However, the standard continuum optical depth τ_{5000} in these layers is greater than 20, and the differences in damping have no significant effect on the line profile calculation.

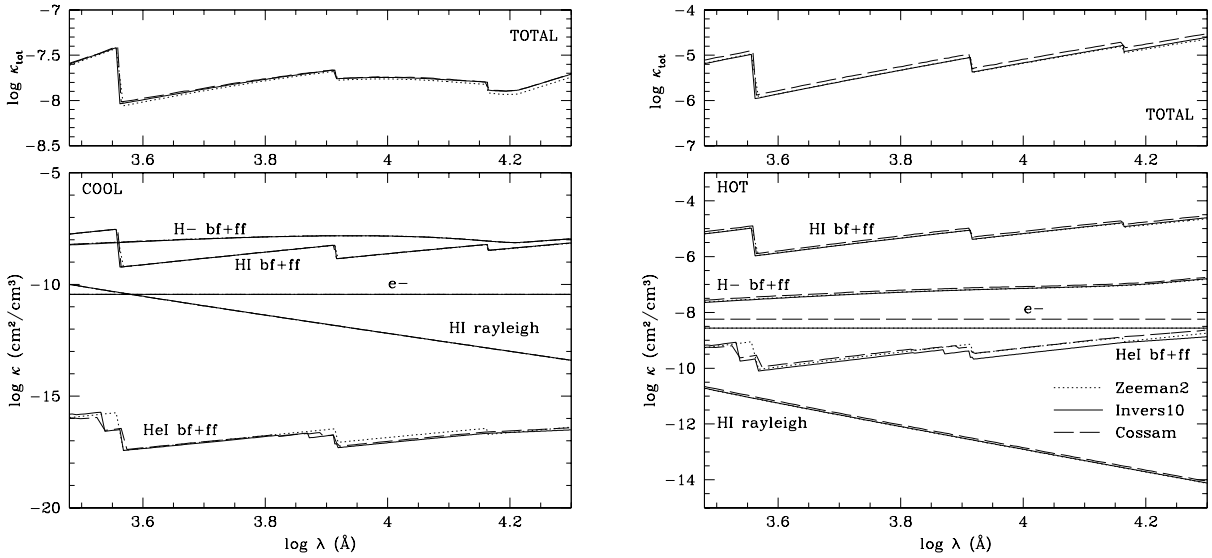

Fig. 1. Continuous opacity distributions for ZEEMAN2, COSSAM and INVERS10. *Left* – selected sources for the "cool" conditions shown in Table 1: *right* – selected sources for the "hot" conditions shown in Table 1. The upper frames show the total opacity for the three codes due to all calculated sources.

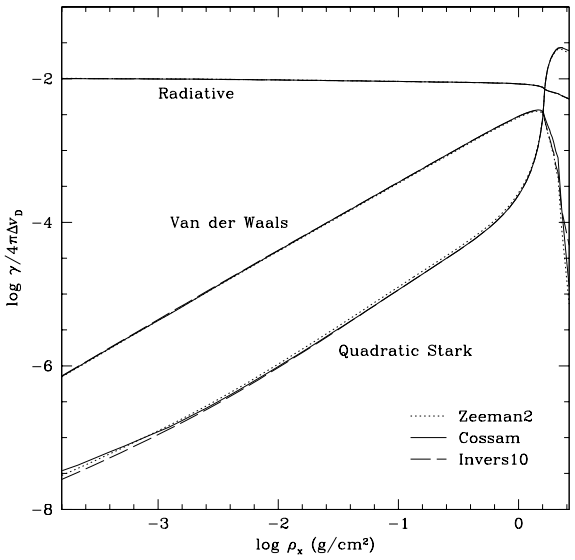

Fig. 2. Radiative, van der Waals and quadratic Stark effect damping coefficients for Fe II λ4923.9 versus column mass, calculated for all levels of the test model atmosphere.

4. Spectrum synthesis for identical input conditions

Having explored the uncertainties resulting from the basic physical data necessary for the synthesis, we now examine the agreement among synthetic Stokes profiles.

4.1. Surface intensities: Local profiles

A comparison of the emergent Stokes profiles calculated at a single point on the stellar surface, characterised by a single uniform magnetic field vector, provides us with the most stringent test of the results of the transfer calculations. We have performed a variety of such tests for Fe II λ4923.9, for null, weak and strong magnetic fields with various orientations, as well as for various surface positions (limb angles) and Fe abundances. The quantitative agreement among the local profiles is summarised in Table 3.

4.1.1. Null magnetic field scenario

Our first comparison examines the agreement of the calculated line profiles in the absence of a magnetic field, for various values of the abundance $\epsilon_{\rm Fe} = \log n_{\rm Fe}/n_{\rm tot}$, at the centre of the stellar disc ($\theta = 0^\circ \rightarrow \mu = \cos\theta = 1.0$). Such a test should most clearly show any effects resulting from the differences in continuous opacity and damping discussed in the previous section. Results of this test are illustrated in Fig. 3.

Each frame in Fig. 3 shows the calculated profiles of Fe II λ4923.9 for zero magnetic field and a given abundance in a lower subframe (which we will call the *profile frame*), along with the pairwise differences among the three calculations in the upper subframe (which we will call the *difference frame*). Differences in continuous opacity and damping notwithstanding, the calculated profiles agree remarkably well, at the level of about 0.1% rms of the continuum intensity $I_{\rm c}$ for all tests.

Similar comparisons were performed for profiles calculated at various limb angles ($\theta = 15^\circ, 30^\circ, 60^\circ$). Profiles for all limb angles show levels of agreement similar to those described above.

This first test establishes that local Stokes I profiles, calculated by the three codes, for Fe II λ4923.9 at various points on the stellar disc, are essentially identical throughout a range of abundance spanning at least 5 dex.

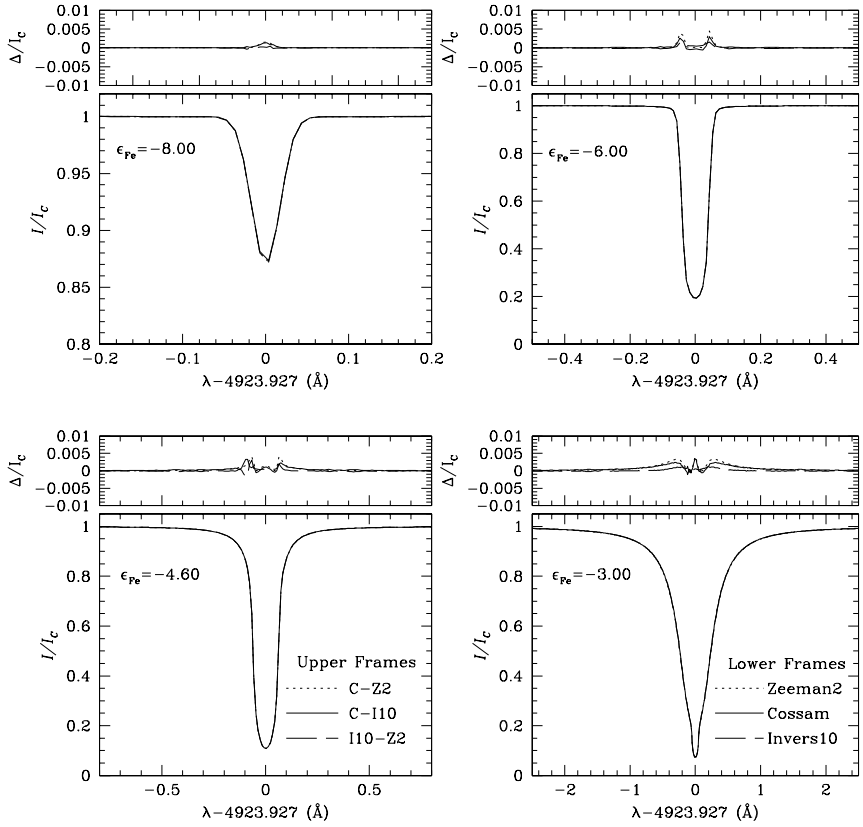

Fig. 3. Local disc-centre profiles of Fe II λ4923.9 calculated for zero magnetic field and four abundances: $\log n_{\rm Fe}/n_{\rm tot} = -8.0, -6.0, -4.6$ and -3.0. The larger lower frames (*profile frames*) compare the profiles calculated by INVERS10, COSSAM and ZEEMAN2, while the smaller upper frames (*difference frames*) show their pairwise differences COSSAM-ZEEMAN2, COSSAM-INVERS10 and INVERS10-ZEEMAN2. Ordinate is in units of the continuum intensity $I_{\rm c}$.

4.1.2. Magnetic field

For abundances $\epsilon_{\rm Fe} = -8.0$ and -4.6 we have compared the calculated local Fe II λ4923.9 Stokes profiles from the three codes for three values of the local magnetic field strength $B = 0.1, 5, 20$ kG, as well as for three values of the magnetic field orientation, $(\psi, \phi) = (0°, 0°), (40°, 0°), (90°, 0°)$ (where ψ and ϕ are respectively the polar and azimuthal angles of the magnetic field vector as described by Landolfi et al. 1993). To illustrate the results of these tests we show in Fig. 4 the calculations for magnetic field orientation $(\psi, \phi) = (40°, 0°)$ and an Fe abundance $\epsilon_{\rm Fe} = -4.6$.

The Stokes I profiles calculated by the three codes and shown in Fig. 4 show levels of agreement similar to those obtained for the respective nonmagnetic case. Stokes V, Q and U profiles agree to within 1% rms of their full amplitudes.

To facilitate explicit comparison with these calculations, we tabulate the Stokes profiles shown in Fig. 4 in Table 4, available only in electronic form at the CDS via anonymous ftp to `cdsarc.u-strasbg.fr (130.79.128.5)` or via

`http://cdsweb.u-strasbg.fr/cgi-bin/qcat?JA+A/374/265`.

This second test establishes that local Stokes I profiles calculated by the three codes, for Fe II λ4923.9 under the influence of a magnetic field, maintain the level of agreement obtained in the case of a null field, and that the associated Stokes V, Q and U profiles agree to within 1% rms of their respective amplitudes, throughout a range of field strengths from 0.1 to 20 kG.

4.2. Surface fluxes: Disc-integrated profiles

It is the Stokes I, Q, U and V flux profiles, obtained by weighting and integrating the local profiles over the stellar disc, that will be ultimately compared with spectropolarimetric observations. From this standpoint flux profiles represent the most important test of the agreement of the three synthesis codes. In this section we compare calculated disc-integrated profiles for both non-magnetic and magnetic scenarios. A quantitative summary of this comparison is provided in Table 5.

4.2.1. Null magnetic field scenario

As in the local case, we begin with a comparison of profiles calculated in the absence of a magnetic field. Such a comparison includes the effects of the (very small) differences in the local profiles established in Sect. 4.1, but furthermore examines the accuracy of the disc integration. Profiles have been calculated for Fe II λ4923.9 for the adopted model atmosphere, abundance $\epsilon_{\rm Fe} = -4.60$, and assuming projected rotational velocities ($v_{\rm e} \sin i$) of 0, 20, 40 and 80 km s^{-1}.

Agreement for $v_{\rm e} \sin i = 0$ km s^{-1} is at the sub-0.1% rms level, and is essentially the same as that observed for local profiles calculated for this abundance. For increasing $v_{\rm e} \sin i$ the absolute level of agreement improves somewhat. We point out that, were these calculations convolved with an instrumental profile (as would commonly be performed for comparison with real observations), small-scale structure in the pairwise differences frames (resulting from

Table 3. Local profile calculations summary. Summary of root mean square (rms) and maximum pairwise deviations for calculations with $\psi = 40°$, $\phi = 0°$. Considering all pixels with intensity lower than 1% of maximum Stokes I profile depth. First value is rms deviation, second is maximum deviation. Values in brackets are full amplitude of the respective profile and the full amplitude expressed in units of the maximum deviation. *Values are in percent of* I_c.

Model	$\epsilon_{Fe} = -8.0$	$\epsilon_{Fe} = -6.0$	$\epsilon_{Fe} = -4.6$	$\epsilon_{Fe} = -3.0$
0 kG	0.070 0.155 (12.8,83)	0.134 0.455 (80.7,177)	0.091 0.404 (89.2,221)	0.095 0.405 (92.8,229)

Model	I	V	Q	U
		$\epsilon_{Fe} = -4.6$		
0.1 kG	0.084 0.381 (89.2,234)	8.99E-3 6.48E-2 (8.00,123)	2.57E-4 1.89E-3 (0.057,30)	3.07E-4 2.48E-3 (0.051,21)
5 kG	0.055 0.242 (82.2,216)	3.36E-2 1.42E-1 (72.2,508)	1.17E-2 4.47E-2 (11.0,246)	4.73E-3 1.67E-2 (1.96,117)
20 kG	0.085 0.422 (77.3,184)	6.10E-2 4.58E-1 (81.2,177)	4.59E-2 6.25E-1 (26.4,42.2)	3.20E-2 4.43E-1 (12.9,29.1)
		$\epsilon_{Fe} = -8.0$		
0.1 kG	0.019 0.043 (12.8,298)	3.62E-3 7.23E-3 (1.31,182)	5.98E-5 1.61E-4 (0.023,143)	2.54E-6 6.24E-6 (1.16E-4,19)
5 kG	0.020 0.043 (3.62,84)	1.70E-2 4.14E-2 (6.98,169)	7.55E-3 1.95E-2 (2.48,127)	2.43E-4 6.01E-4 (1.96E-2,33)
20 kG	0.009 0.036 (2.78,77)	7.96E-3 3.46E-2 (5.34,148)	3.29E-3 1.10E-2 (1.61,148)	2.28E-5 8.42E-5 (2.67E-3,31.7)

Table 5. Disc integrated profile calculations summary. Summary of root mean square (rms) and maximum pairwise deviations. Considering all pixels with intensity lower than 1% of maximum Stokes I profile depth. First value is rms deviation, second is maximum deviation. Values in brackets are full amplitude of the respective profile and the full amplitude expressed in units of the maximum deviation. *Values are in percent of* I_c. For the 4915-4930 Å calculation, "homogeneous" and "heterogeneous" refer to calculations performed with/without verifying identical partition functions and ionisation potentials.

Model	I
0 kG, $v_e \sin i = 0$ km s^{-1}	7.39E-2 3.25E-1 (87.6,270)
0 kG, $v_e \sin i = 20$ km s^{-1}	4.72E-2 1.57E-1 (27.8,177)
0 kG, $v_e \sin i = 40$ km s^{-1}	3.41E-2 1.35E-1 (14.7,109)
0 kG, $v_e \sin i = 80$ km s^{-1}	2.68E-2 8.44E-2 (7.54, 89)

Model	I	V	Q	U
		$v_e \sin i = 20$ km s^{-1}, dipole field with $B_d = 5$ kG		
$f = 0°$	4.43E-2 1.03E-1 (40.2,390)	1.67E-2 6.60E-2 (9.6,146)	6.46E-3 2.99E-2 (1.7,57)	4.59E-3 1.87E-2 (1.7,91)
$f = 120°$	4.46E-2 1.42E-1 (39.5,278)	1.57E-2 6.84E-2 (9.8,143)	4.52E-3 2.00E-2 (1.4,70)	7.81E-3 3.31E-2 (1.9,57)
$f = 240°$	4.38E-2 1.34E-1 (39.5,295)	2.05E-2 9.74E-2 (9.8,101)	5.21E-3 1.75E-2 (1.4,80)	7.69E-3 3.32E-2 (1.9,57)
		4915–4930 Å, $v_e \sin i = 20$ km s^{-1}, $B_d = 5$ kG		
heterogeneous	7.74E-2 2.13E-1	2.64E-2 9.76E-2	1.39E-2 5.45E-2	6.80E-3 3.50E-2
homogeneous	3.10E-2 1.04E-1	1.70E-2 6.04E-2	1.16E-2 4.40E-2	8.92E-3 5.60E-2

differences in the disc integration grids employed by the three codes) would essentially disappear, and the agreement would improve correspondingly.

4.2.2. Magnetic field

We have also compared disc-integrated profiles of Fe II λ4923.9 calculated assuming a dipolar surface magnetic field configuration, observed from three different aspects (i.e. at three difference rotational phases f). The profiles correspond to $\epsilon_{Fe} = -4.60$ and $v_e \sin i = 20$ km s^{-1}. Agreement among the Stokes I profiles is similar to that obtained in the null field case (better than 0.05% rms, corresponding to agreement to better than 0.2% of the profile depth), while agreement for Stokes V is at the level of 0.02% rms (0.2% of the profile full amplitude), and Stokes Q/U agree at the sub-0.01% rms level (0.4% of the profile amplitude).

These tests establish that the differences in disc-integrated Stokes profiles of Fe II λ4923.9 calculated by the three codes, for homogeneous input conditions, both in the presence and absence of a magnetic field, remain at or below the levels of agreement obtained for local Stokes profiles. The observed levels of agreement for disc-integrated Stokes V, Q and U profiles all correpond to congruence to within better than 1% rms of the profile

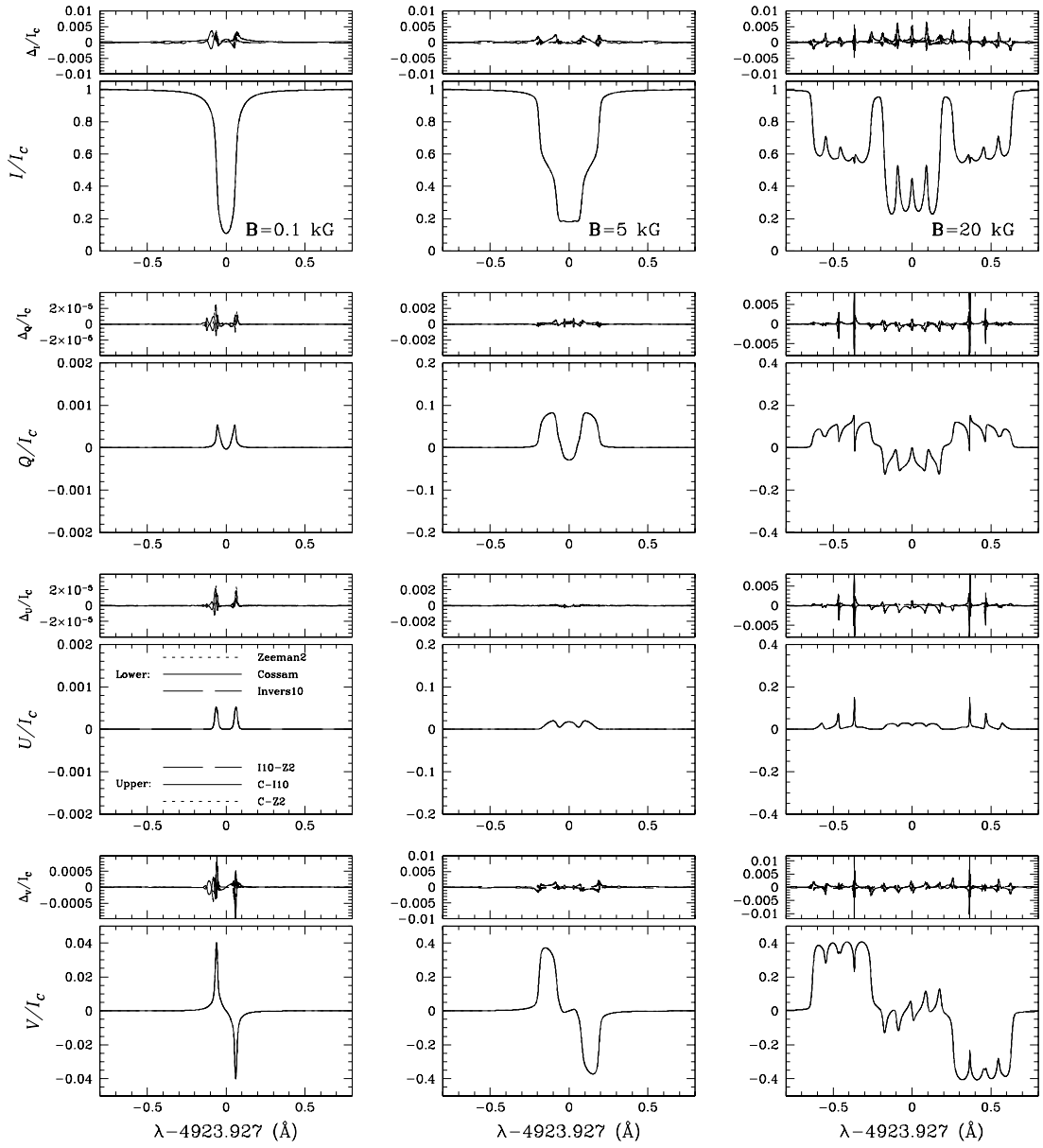

Fig. 4. Local disc-centre profiles of Fe II λ4923.9 for abundance $\epsilon_{\rm Fe} = -4.6$ calculated for 0.1, 5.0 and 20.0 kG magnetic field strengths, with orientation $\psi = 40°$, $\phi = 0°$. The vertical scale of the small upper difference frames for Stokes Q, U and V corresponds to 2% of that of the respective larger lower profile frame. Note the different scales for the different Stokes parameters and field strengths.

amplitude, and this agreement is maintained for various field configurations.

Is such good agreement maintained in the more realistic case of synthetic spectrum calculated including multiple blended ions? To answer this question we have compared calculations of the spectral region 4915–4930 Å, including the effects of 34 spectral lines formed by 12 different ions (with data obtained from the VALD database), as well as a dipolar magnetic field. This comparison is illustrated in Fig. 5. Our first such calculations showed important systematic differences between ZEEMAN2 and the other codes, especially for Stokes I (up to more than 1% of $I_{\rm c}$). Some of these differences were found to be due to differences in adopted partition functions and, for trace ions (e.g. Fe I), very small differences in adopted ionisation potentials. (These differences trace the close connection of COSSAM and INVERS10 to Kurucz's ATLAS codes and data, and the lack of such a connection for ZEEMAN2.) After homogenising partition functions and relevant ionisation potentials, the systematic differences essentially disappeared, but obvious differences still remained for a few apparently unrelated lines. This can be seen in Fig. 5. (e.g. Fe I λ4918.0, Fe I λ4918.9, Fe I/II + Cr I λ4922.2). Examination of spectra calculated for this wavelength region for null magnetic field, as well as examination of the experimental versus LS coupling Landé factors for these lines, showed clearly that these discrepancies result from frequent differences between observed and

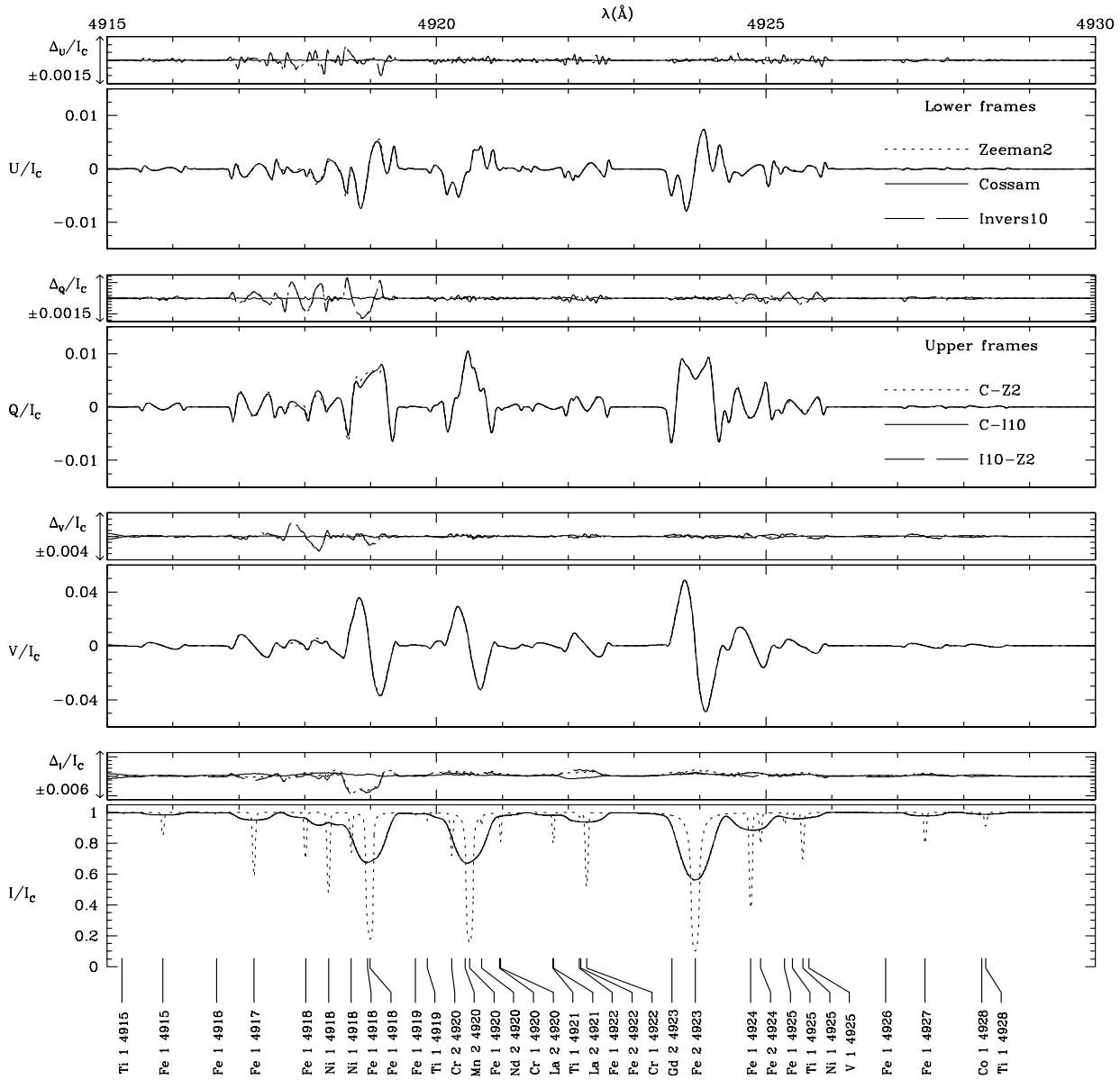

Fig. 5. Synthetic disc-integrated spectrum for the region 4915–4930 Å, including the effects of 34 spectral lines (identified at bottom). The abundance table is solar, the magnetic field is dipolar with $B_{\rm d} = 5$ kG, $i = 90°, \beta = 45°, \Theta = 0°$ and $f = 0°$. The projected rotational velocity is $v_{\rm e} \sin i = 20$ km s^{-1}. The disc-centre spectrum, calculated in the absence of a magnetic field by Cossam, has been overlayed on Stokes I to clarify the distribution of spectral lines. Nearly all of the visible structure in the difference frames results from Landé factor discrepancies.

calculated Landé factors (e.g. as large as a factor of two for Fe I λ4918.0). The remaining differences in Fig. 5 are therefore a direct consequence of the (clearly hazardous) Zeeman2 strategy of calculating Landé factors.

This test shows that, apart from differences resulting from calculated versus experimental Landé factors, the codes continue to maintain good agreement even for calculations including various blended ions.

5. Discussion

The comparisons performed in Sect. 4 show, for identical input data, that the differences between Stokes profiles calculated using Cossam, Invers10 and Zeeman2 are sufficiently small so as to allow for congruent interpretation of the highest quality stellar Stokes $IQUV$ data presently available ($S/N \lesssim 1000$, $\lambda/\Delta\lambda \simeq 35\,000$). As the next generation of high-resolution spectropolarimeters (such as the ESPaDOnS instrument; Donati et al. 1998) begin to see light on medium- and large-class telescopes this situation will remain unchanged for all but the brightest sources. Therefore our basic ability to solve the PRT problem and to calculate precise disc-integrated Stokes $IQUV$ profiles is not an important limitation for modeling observations. This is the primary conclusion of this paper.

On the other hand, as is aptly illustrated in Sect. 4.2.2, uncertainties in input atomic and astrophysical data can have an important impact on the shapes and amplitudes of Stokes profiles. Atomic data are often subject to important errors: gf-values, Landé factors, Zeeman component intensities, damping coefficients, partition functions, and excitation and ionisation potentials all exhibit uncertainties of varying degree. Even more important are uncertainties in the input astrophysical data, particularly the state and structure of the model stellar atmosphere. Such uncertainties are especially critical for magnetic stars: surface features (starspots on cool stars, abundance nonuniformities on tepid stars) indicate that no single model of the vertical run of temperature and pressure is valid at all stellar surface locations. The convective state of magnetic atmospheres is uncertain due to possible suppression of velocity fields by the magnetic field. The atmospheric chemical composition of magnetic tepid stars is frequently strongly nonsolar, and elements may furthermore be strongly stratified; a unique abundance of each chemical element may not characterise all atmospheric depths (let alone all surface locations). Although the impact of these physical complexities is widely recognised, they are not generally included in stellar atmosphere models (but see Piskunov & Kupka 2001 for some steps in this direction). In fact, the overwhelming majority of line profile modeling to date (polarised and unpolarised) has been accomplished using atmosphere models characterised by scaled solar abundance tables.

Of course, all of these unaccounted-for model atmosphere errors contribute to errors in calculated Stokes profiles (errors which can potentially be very much larger than those discussed in Sect. 4). Such profiles are frequently used to recover stellar magnetic field topologies by comparing the calculations with observations. A number of such modeling strategies are presently under development. For example, Bagnulo & Wade (2001) are attempting to fit Stokes $IQUV$ profile variations within the context of a low-order multipolar framework. Kochukhov et al. (2001), on the other hand, employ a method based on Doppler Imaging principles to accomplish the same goal. At this point, it is not clear to what degree uncertainties in calculated Stokes profiles may lead to an inability to accurately reproduce observed profiles or to inaccurate recovery of the parent magnetic field. Neither is it clear how this will depend on the modeling strategy employed.

Therefore, while we have shown that Stokes $IQUV$ profiles of magnetic stars can in principle be calculated to very high precision, in practice this agreement means little in terms of the accuracy of such profiles, which will be limited overwhelmingly by uncertainties in input atomic and astrophysical data, in particular model stellar atmospheres.

Acknowledgements. GAW acknowledges support during 1998–2000 from the Natural Sciences and Engineering Research Council of Canada (NSERC) in the form of an NSERC postdoctoral fellowship, as well as support from the NSERC operating grants of J. B. Lester and C. T. Bolton (University of Toronto). JDL acknowledges support from NSERC in the form of an operating grant. S. Bagnulo and M. J. Stift gratefully acknowledge financial support by the Austrian *Fonds zur Förderung der Wissenschaftlichen Forschung*, project P12101-AST. Research in scientific programming with Ada has been funded by the *Hochschuljubiläumsstiftung der Stadt Wien*, project *Software Engineering with Ada95.* We thank F. Leone for taking time to provide ATLAS9 continuous opacity calculations.

References

Aller, M. F., & Everett, C. H. M. 1972, ApJ, 172, 447
Auer, L. H., Heasley, J. N., & House, L. L. 1977, ApJ, 216, 531
Bagnulo, S. & Wade, G. A. 2001, in Proceedings of Magnetic Fields Across the H–R Diagram, PASP Conf. Ser., ed. G. Mathys, S. Solanki, & D. Wickramasinghe, in press
Baschek, B., Holweger, H., & Traving, G. 1966, Abh. Hamburger Sternwarte, Band VIII, 26
Babcock, H. W. 1947, ApJ, 105, 105
Babcock, H. W. 1958, ApJ, 128, 228
Bohlender, D. A., Brown, D. N., Landstreet, J. D., & Thompson, I. B. 1987, ApJ, 323, 325
Bolton, C. T. 1970, ApJ, 161, 1187
Bolton, C. T. 1971, A&A, 14, 233
Carbon, & Gingerich, O. 1969, in Theory and Observation of Normal Stellar Atmospheres, 399
Chmielewski, Y. 1979, Publ. Obs. de Genève, Série B, Fasc. 7
Cowley, C. R. 1971, Obs., 91, 139
Cowley, C. R. 1994, Obs., 114, 308
Cowley, C. R. 1998, `ftp://astro.lsa.umich.edu/pub/get/cowley /partition/bolpfn.f`
Cowley, C. R., & Adelman, S. J. 1983, QJRAS, 24, 393
Donati, J. F., Semel, M., Carter, B. D., Rees, D. E., & Cameron, A. C. 1997, MNRAS, 291, 658
Donati, J.-F., Catala, C., & Landstreet, J. D. 1998, in Proceedings of the fifth CFHT user's meeting, 50
Drawin, H. W., & Felenbok, P. 1965, Z. Astrophys., 63, 62
Fensl, R. M. 1995, A&AS, 112, 191
Gingerich, O. 1964, SAO Report #167
Gonzalez, J.-F., Artru, M.-C., & Michaud, G. 1995, A&A, 302, 788
Gray, D. F. 1992, The Observation and Analysis of Stellar Photo spheres (Cambridge University Press)
Griem, H. R., 1968, ApJ, 154, 1111
Hardorp, J., Shore, S. N., & Wittmann, A. 1975, in Proc. IAU Coll. No. 32, Physics of Ap Stars, ed. W. W. Weiss, H. Jenkner, & H. J. Wood, Universitätssternwarte Wien, 419
Humlicek 1982, J. Quant. Spec. Rad. Trans. 27, 437
Irwin, A. W. 1981, ApJS, 45, 621
Johns-Krull, C. M., & Valenti, J. A. 1996, ApJ, 459, 95
Johns-Krull, C. M., Valenti, J. A., & Koresko, C. 1999, ApJ, 516, 900
Kemp, J. C., Swedlund, J. B., Landstreet, J. D., & Angel, J. R. P. 1970, ApJL, 161, 77
Kochukhov, O., Piskunov, N., Ilyin, I., Ilyina, S., & Tuominen, I. 2001, in Proceedings of Magnetic Fields Across the H–R Diagram, PASP Conf. Ser., ed. G. Mathys, S. Solanki, & D. Wickramasinghe, in press

Kurucz, R. 1993, CDROM Model Distribution, Smithsonian Astrophys. Obs.
Landolfi, M., Landi Degl'Innocenti, E., Landi Degl'Innocenti, M., & Leroy, J.-L. 1993, A&A, 272, 285
Landolt-Börnstein 1982, Zahlenwerte und Funktionen aus Naturwissenschaften und Technik, Neue Serie, Gruppe VI: Astronomie, Astrophysik und Weltraumforschung, Band 2, Teilband b, ed. K. Schaifers, & H. H. Voigt, 107
Landstreet, J. D. 1982, ApJ, 258, 639
Landstreet, J. D. 1988, ApJ, 326, 967
Leroy, J.-L. 1995, A&AS, 114, 79
Leroy, J.-L., Landolfi, M., & Landi Degl'Innocenti, E. 1996, A&A, 311, 513
Martin, B., & Wickramasinghe, D. T. 1979, MNRAS, 189, 883
Mathys, G. 1993, A&AS, 108, 547
Mihalas, D. 1970, Stellar Atmospheres
Peytremann, E., Baschek, B., Holweger, H., & Traving, G. 1967, Rapport Interne, Obs. de Genève
Piskunov, N. E., Kupka, F., Ryabchikova, T. A., Weiss, W. W., & Jeffery, C. S. 1995, A&AS, 112, 525
Piskunov, N. 1999, in Proceedings of the 2nd Workshop on Solar Polarisation, ed. J. Stenflo, & K. N. Nagendra, 1998, Bangalore, India (Kluwer Acad. Publ. ASSL), 243, 515
Piskunov, N. E., & Kupka, F. 2001, ApJ, 547, 1040
Putney, A. 1999, in 11th European Workshop on White Dwarfs, ASP Conf. Ser. #169, ed. S.-E. Solheim, & E. G. Meistas, 195
Rees, D. E., Murphy, G. A., & Durrant, C. J. 1989, ApJ, 339, 1093
Rees, D. E. 1987, in Numerical Radiative Transfer, ed. Kalkofen W. (Cambridge University Press), 213
Shurcliff, W. A. 1962, Polarized light (Harvard University Press, Cambridge)
Stehlé, C., & Hutcheon, R. 1999, A&AS, 140, 93
Stift, M. J. 1985, MNRAS, 217, 55
Stift, M. J. 1996, in Model Atmospheres and Spectrum Synthesis, ed. S. J. Adelman, F. Kupka, & W. W. Weiss, ASP Conf. Ser., 108, 217
Stift, M. J. 1998a, Comp. Phys., 12, 150
Stift, M. J. 1998b, in Reliable Software Technologies – Ada-Europe '98, ed. L. Asplund, Lecture Notes in Computer Science, 1411 (Springer), 128
Traving, G., Baschek, B., & Holweger, H. 1966, Abh. Hamburger Sternwarte, Band, VIII, 1
Wade, G. A., Donati, J.-F., Landstreet, J. D., & Shorlin, S. L. S. 2000, MNRAS, 313, 823